N-doped few-layered graphene-polyNi complex nanocomposite with excellent electrochromic properties

Marta Nunes,[a] Mariana Araújo,[a] Revathi Bacsa,[b] Roberta Viana Ferreira,[c] Eva Castillejos,[d] Phillipe Serp[b], A. Robert Hillman[e] and Cristina Freire[a*]

[a] REQUIMTE/LAQV, Departamento de Química e Bioquímica, Faculdade de Ciências, Universidade do Porto, 4169-007 Porto, Portugal

[b] Laboratoire de Chimie de Coordination UPR CNRS 8241, composante ENSIACET, Toulouse Université, 118 route Narbonne, 31077 Toulouse, France

[c] Departamento de Química, Universidade Federal de Minas Gerais, Campus Pampulha, 31270-901 Belo Horizonte, Minas Gerais, Brazil

[d] Grupo de Diseño Molecular de Catalizadores Heterogéneos, C/ Marie Curie, 2, Cantoblanco, Madrid, E-28049 Spain

[e] Department of Chemistry, University of Leicester, Leicester LE1 7RH, United Kingdom

* Corresponding author: Dr. Cristina Freire; e-mail: acfreire@fc.up.pt.

Tel.: +351 22 04020590; Fax: +351 22 0402 695.

ABSTRACT

A new nanocomposite was obtained through the incorporation of N-doped few layer graphene (N-FLG) into films of the electroactive polymer poly[Ni(3-Mesalen)] (poly[1]). The nanocomposite, N-FLG@poly[1], prepared by *in situ* electropolymerization, showed similar electrochemical responses to pristine poly[1], but with more well-defined redox peaks and higher current intensities, in compliance with larger electroactive surface coverage. N-FLG incorporation did not affect the electronic structure of poly[1], but decreased in 12 % the molar extinction coefficient of the charge transfer band between metal and oxidized ligand, which is a promising advantage since this band is related to polymer degradation.

The N-FLG@poly[1] showed multi-electrochromic behaviour (yellow in reduced state and green / russet in oxidised states) and revealed excellent improvement in electrochromic performance compared to original poly[1], specifically an increase of 71 % in electrochemical stability (loss of 2.7% in charge after 10 000 switching cycles). Furthermore, nanocomposite formation decreased the switching time for oxidation (reduction) τ = 9 s (11 s) and improved the optical contrast (ΔT = 35.9%; increase of 38%) and colouration efficiency (η = 108.9 cm^2 C^{-1}; increase of 12 %), for a representative film of coverage Γ = 296 nmol cm^{-2}. The excellent electrochromic performance improvements are attributed to the alternative conducting pathways and to morphological modifications induced by N-FLG.

1. INTRODUCTION

Electrochromic (EC) materials typically comprise redox-active species which exhibit significant, lasting and reversible changes in color upon the injection or withdrawal of electrons [1]. The incorporation of these materials in EC devices has attracted a great deal of attention due to potential applications, such as in intelligent optical displays, rear-view mirrors (automotive industry) and energy-saving smart windows [2,3].

Among EC materials, conducting polymers (CPs) are very attractive, mainly due to their cost effectiveness, high optical contrast and multichromism [4,5]. Nonetheless, improvements in electrochemical stability, electrochromic contrast and switching times remain priority requirements for their successful application [6]. In order to achieve these goals, composites of CPs with nanostructures have been prepared [7-9]; these new polymeric nanocomposites (PNCs), are functional hybrid materials that typically comprise a nanometric filler, and show considerable improved properties due to synergic effects between the components [10-12].

Due to its conjugated structure, excellent electron-transport properties and versatile chemistry, graphene (G) has emerged as one of the most attractive carbon nanomaterials to be combined with CPs. With a two-dimensional (2D) sp^2-hybridized carbon structure in a single-atom-thick sheet, graphene shows interesting physicochemical properties, such as a large theoretical specific surface area, high carrier mobility at room temperature, good thermal conductivity, high Young's modulus and good optical transmittance [13-15]. Several graphene/PNCs have been prepared to optimize the properties and performances of polymers for several applications, such as in supercapacitors [16-18], fuel [19,20] and solar [21] cells, sensors [22,23] lithium-ion batteries [24] and in anticorrosion coatings [25]. For EC applications, some graphene/CPs nanocomposites

with enhanced EC properties have also been reported, combining polyaniline (PANI) and pyrrole-derivatives with graphene [4,26], sulfonated-graphene [27], graphene oxide [28] or reduced graphene oxide [6], as counterparts. Ma *et al.* [1] reported the preparation of an electrochromic polyschiff base functionalised with reduced graphene oxide.

More recently, the chemical doping of graphene with heteroatoms (nitrogen, boron and sulphur) has emerged as an important approach to tailor the electrical, morphological and chemical properties of pristine graphene. Nitrogen is the most commonly used dopant, mainly due to its similar atomic radius to carbon, which prevents significant lattice mismatch [29,30]. The main differences between nitrogen-doped graphene (N-G) and pristine graphene are (i) the spin density and charge distribution on the carbon atoms (influenced by the neighbour nitrogen dopants) and (ii) the open band gap, making N-G an n-type semiconductor [31], which is very useful for nanoelectronic applications. In the electrochromism field, the application of a N-G/TiO_2 nanocomposite, as an efficient electrode material to improve the EC properties of polythiophene-derivative EC polymer was reported [32].

This work reports the preparation of a novel PNC made from poly[Ni(3-Mesalen)] electroactive film, designated hereafter as poly[1], and nitrogen-doped few layer graphene (N-FLG), and the evaluation of its EC performance. The study of the EC performance of the pristine poly[1], described elsewhere [33], revealed promising EC properties, with good electrochemical stability and interesting colour changes from yellow in neutral state to green and russet (reddish-brown) in oxidized states. The preparation of the nanocomposite between poly[1] and pristine graphene flakes (GF) [34] allowed a good improvement in the EC properties, leading to more favourable switching times and better optical modulation and electrochemical stability relatively to original poly[1]. The fundamental advance reported here is that a novel PNC, N-FLG@poly[1],

prepared by *in situ* electropolymerization of poly[1] in the presence of N-FLG allowed the resulting nanocomposite to clearly surpass the conductive and electrochromic properties of both pristine poly[1] and the nanocomposite with GF; the implication is that N-doping of few layer graphene, prepared by CVD using a literature adapted methodology, had a unique beneficial effect. To the best of our knowledge, this is the first study on PNCs from the group of Metal-*salen* type electroactive metallopolymers and nitrogen-doped graphene.

2. EXPERIMENTAL SECTION

2.1 Materials and instrumentation

The complex *N,N'*-bis(3-methylsalicylideneiminate) nickel(II), [Ni(3-Mesalen)], and the relevant *salen* ligand were prepared as described in the literature [35]. Acetonitrile and propylene carbonate (PC) (Romil, pro analysis grade) and $LiClO_4$ (Aldrich, 99 %) were used as received. Ethylene and ammonia gases using in N-FLG preparation were obtained from Air Liquid, France. N-FLG was prepared by modifying our previously developed procedure for few layer graphene, as detailed in section 2.2 [36].

X-ray photoelectron spectroscopy (XPS) measurements were performed at CEMUP (Porto, Portugal), in a Kratos AXIS Ultra HSA spectrometer with a monochromatic Al Kα radiation (1486.7 eV), using the polymeric films or pellets of the nanomaterial (N-FLG). The raw XPS spectra were deconvoluted with the XPSPEAK 4.1 software, using a non-linear least squares fitting routine after a Shirley-type background subtraction. To correct for possible deviations caused by sample charging, the C1s peak at 284.6 eV was taken as an internal standard. The surface atomic percentages were calculated from the corresponding peak areas, using sensitivity factors provided by the manufacturer.

Scanning Electron Microscopy / Energy-Dispersive X-Ray Spectroscopy (SEM/EDS) analyses were performed at CEMUP (Porto, Portugal), using a High Resolution (Schottky) Environmental Scanning Electron Microscope with X-Ray Microanalysis and Electron Backscattered Diffraction analysis (Quanta 400 FEG ESEM / EDAX Genesis X4M).

Transmission Electron Microscopy (TEM, JEOL 1400) was used to study the morphology of the N-FLG samples; Raman spectroscopy (HR 800 Jobin Yvon Horiba, micro spectrometer using the red line of an argon laser, λ = 639 nm, as an excitation source) was used to study the structure of both FLG and N-FLG. Chemical analysis was carried out in STEM configuration (spot mode, probe diameter = 1 nm) using a Bruker EDAX spectrometer (provided with a Silicon Drift Detector with a resolution 127 eV).

Electrochemical studies were performed using an Autolab PGSTAT 30 potentiostat/galvanostat (EcoChimie B.V.), controlled by a GPES software.A three-electrode and separate compartment cell, enclosed in a grounded Faraday cage, was used with an Ag/AgCl (NaCl / 1.0 mol dm^{-3}) electrode (Metrohm ref. 6.0724.140) as the reference electrode, a Pt plate as the counter electrode and poly(ethylene terephthalate) (PET) coated with indium tin oxide (ITO) (ITO/PET) (Aldrich, resistivity of 60 Ω sq^{-1}) as the working electrode. Coulometric measurements used a Pt disk working electrode (area 0.0314 cm^2, BAS), previously polished with aluminium oxide of particle size 0.3 μm (Buehler) on a microcloth polishing pad (Buehler), then washed with ultra-pure water (resistivity 18.2 MΩ cm at 25°C, Millipore) and finally CH_3CN.

The spectroelectrochemical studies were performed *in situ* using an Agilent 8453 spectrophotometer (with diode array detection) coupled to the potentiostat/galvanostat. The experimental set up consisted up a teflon cell with an Ag/AgCl (NaCl / 3.0 mol dm^{-}

^{3}) (Bio-Logic) reference electrode, a Pt grid counter electrode and an ITO/PET (typical area 0.785 cm^2) as working electrode.

2.2 N-FLG preparation and characterization

N-FLG was prepared by CVD process, adapting a procedure reported elsewhere for the synthesis of few layer graphene (non-doped) [36]. Briefly, few layer graphene was produced by the catalytic chemical decomposition of a mixture of ethylene and hydrogen gas in a vertical fluidized bed reactor at 650 ºC, in the presence of a cobalt ferrite spinel catalyst. Few layer graphene flakes were separated from the catalyst by dissolving the latter in 65% hydrochloric acid at 25°C. Nitrogen doping was achieved by replacing pure ethylene by a mixture of ethylene and ammonia (90:10) under the same conditions. Both FLG and N-FLG powder was recovered after washing with 35 % HCl at 25°C. The nitrogen content was determined from both chemical analysis and XPS. The structure of the as-prepared N-FLG was confirmed from TEM and Raman spectroscopy.

2.3 Film preparation and electrochemical characterization

The N-FLG@poly[1] nanocomposite films were prepared by cyclic voltammetry (CV) from the corresponding monomer solution, 1.0 mmol dm^{-3} [Ni(3-Mesalen)] complex in 0.1 mol dm^{-3} $LiClO_4/CH_3CN$, containing 0.5 wt.% (N-FLG/[Ni(3-Mesalen)] wt.%) of N-FLG. The potential of the working electrode (ITO/PET 3.0 cm^2) was cycled between -0.2 and 1.3 V, at a scan rate v = 0.100 V s^{-1}, for 30 scans; other conditions are specified in the relevant text. Prior to electrodeposition, the starting solution was refluxed for 3 hours, followed by sonication for 10 min, to ensure an optimum dispersion of the N-FLG powder and to promote interaction between the monomer and N-FLG (e.g.

adsorption of monomer on N-FLG). Pristine poly[1] films were prepared using the same experimental conditions but without N-FLG in the deposition solution.

After film deposition, the modified electrodes were rinsed with CH_3CN, immersed in a monomer- and N-FLG-free 0.1 mol dm^{-3} $LiClO_4$/PC solution and cycled (by CV) in the potential range -0.2 to 1.3 V, at v = 0.010 V s^{-1}.

The electroactive surface coverage, Γ / nmol cm^{-2} (cited in terms of monomeric units), of each film was determined by a coulometric assay [37,38], using cyclic voltammograms (CVs) obtained in monomer-free 0.1 mol dm^{-3} $LiClO_4/CH_3CN$ solution at a slow scan rate (v = 0.010 V s^{-1}) to ensure complete film redox conversion. The variation of coverage, Γ (strictly, the number of accessible redox sites on the chosen timescale; see below), with the number of electrodeposition cycles was studied for films prepared with 1 - 50 cycles. The doping level (n) value used for Γ determination was calculated from comparison of coulometric data for film deposition and cycling, an established procedure in the literature [33,34,37]; the outcome here was a value of n = 0.65.

2.4 Composition and morphological characterization

The composition and morphology of the nanocomposite films were characterized by XPS and SEM/EDS, respectively, by the analysis of films in the reduced state (E = -0.2 V, after cycling the potential between -0.2 and 1.3 V at v = 0.010 V s^{-1}, for 2 scans, in $LiClO_4/CH_3CN$). Exceptionally, in the preparation of nanocomposite for SEM/EDS analysis, the percentage of N-FLG used in the deposition solution was increased to 25 wt.%, in order to make the N-FLG flakes more readily observable in the polymeric matrix.

2.5 Spectroelectrochemical studies

In the monitoring of the film redox switching by *in situ* UV-Vis spectroscopy, the potential was cycled between -0.2 and 1.3 V, at v = 0.020 V s^{-1}, using 0.1 mol dm^{-3} $LiClO_4$/PC as the supporting electrolyte. The UV-Vis spectra were acquired simultaneously at 0.5 s intervals, in the wavelength range 315 - 1100 nm. The molar extinction coefficients, ε / cm^{-1} mol^{-1} dm^3, of all electronic bands were calculated using the combination of the Beer-Lambert and Faraday laws [37-39] (Equation 1):

$$Abs(\lambda) = \varepsilon(\lambda)\, Q / nFA \qquad (1)$$

where Q is the charge (C), n is the doping level (see above), F is the Faraday constant and A the electrode area (cm^2).

2.6 Evaluation of electrochromic properties

The evaluation of the EC parameters was performed for films exposed to 0.1 mol dm^{-3} $LiClO_4$/PC supporting electrolyte, for the yellow ↔ green redox transition, using an established procedure [33]. The electrochemical stability tests involved repetitive double potential step chronoamperometry. Each cycle comprised two sequential potential steps, to E = 0.0 and 0.6 V, each of duration 50 s. The full test involved 9815 redox cycles (≈ 12 days). The switching times were determined as the time taken for 85% of the full current intensity change [34], once the correspondence between switching times determined from peak current intensity and optical change was already reported for pristine poly[1] [33]. The remaining EC parameters were determined by *in situ* monitoring of chronoamperometric and chronoabsorptometric responses, where the latter involved acquisition of UV-Vis spectra at intervals of 1 s, during the course of 4 redox cycles; single wavelength data focused on the absorption at λ = 820 nm.

The change of the optical density, ΔOD, (or optical absorbance change, ΔAbs), was calculated using Equation 2 [40]:

$$\Delta Abs\ (\lambda) = \Delta OD\ (\lambda) = \log\ (T_{red}(\lambda)\ T_{ox}(\lambda)) \quad (2)$$

where T_{red} and T_{ox} are the transmittance values of the polymeric films in reduced and oxidized states, respectively, at λ = 820 nm. The colouration efficiency (η / $cm^2\ C^{-1}$) was calculated from the relation between ΔOD and the amount of injected/ejected charge per unit area, Q_d, required to induce complete optical switching, given by Equation 3 [40,41]:

$$\eta = \Delta OD / Q_d \quad (3)$$

Corresponding EC parameters were also evaluated for pristine poly[1] film under the same conditions, for comparison purposes.

3. RESULTS AND DISCUSSION

3.1 N-FLG characterization

The SEM, TEM and high resolution images confirming the structure of undoped FLG obtained by catalytic CVD are shown in Figure S1 in Supporting Information (SI). The details on the structure of the material including thickness determination and stacking disorder are given in our previous article [36]. On replacing ethylene by ethylene + ammonia, it was observed that the yield of carbon deposition was reduced by over 80% as compared to pure ethylene. Figure 1 shows the TEM images of (a) purified N-FLG and (b) an enlarged view of the edge of a flake. The microscopy images show the presence of uniform flakes of around 200 nm. The edges of the flakes showed increased exfoliation and appeared more transparent. An enlarged view of the edge shows curling of the edges. It has been reported in the literature that doping occurs preferentially at graphene edges [42]. TEM high-resolution image of the N-FLG surface (Figure 1 (d)) shows the lattice fringes corresponding to graphite structure, in agreement with the hexagonal pattern

characteristic of a graphitic structure, given in the insets. Different areas in the sample showed different FFT patterns and in certain regions, underlying graphene planes rotated with respect to the top graphene layer could be seen. This observation indicates that N-FLG structure is similar to the undoped FLG structure in having graphene layers stacked randomly [36], even though this could not be confirmed from Raman spectra due to the weak 2D band, see below. Figure 1 (d) shows the high resolution image of a flake edge, where significant disorder is seen.

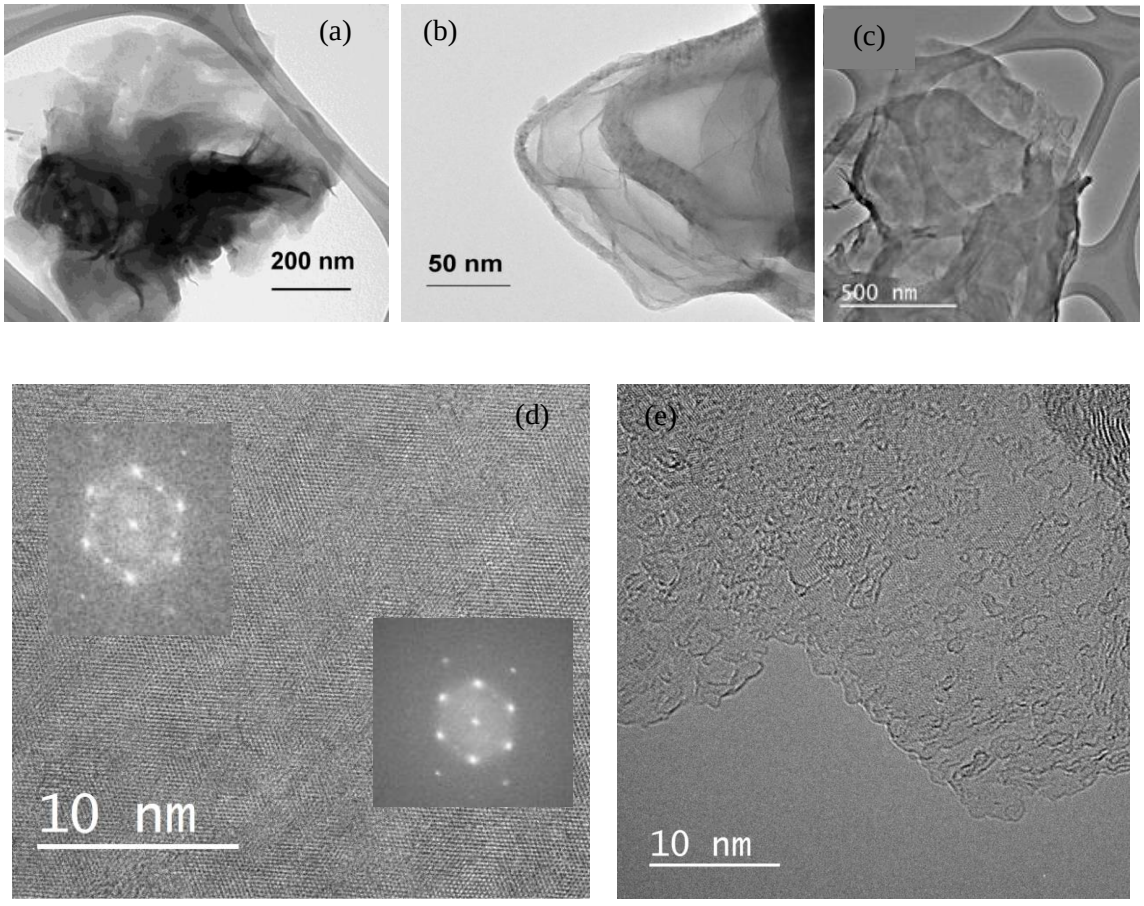

Figure 1. TEM images of purified N-FLG: (a) N-FLG flakes, (b) edge of a flake, (c) a single flake, (d) high-resolution image of the N-FLG surface, with the Fourier transformed image showing the hexagonal pattern characteristic of a graphite structure and a local Fourier transformed image showing other graphene layers rotated with respect to the first layer in the inset, and (e) high resolution image of a flake edge.

The nitrogen content of N-FLG as determined from chemical analysis was found to be ~ 2.8 %. XPS was further used to confirm the presence of nitrogen in the sample. The deconvoluted high-resolution spectra of the identified elements are presented in Figure 2.

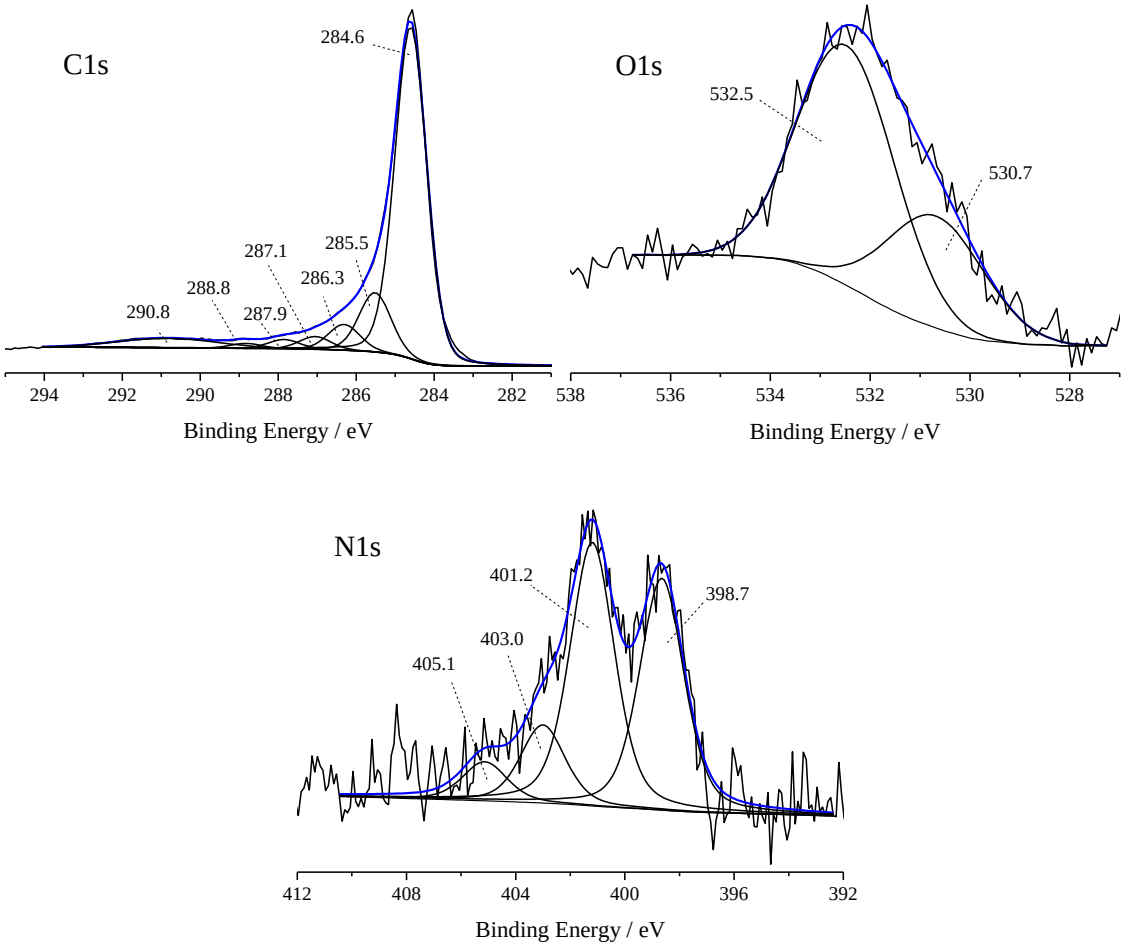

Figure 2. High-resolution XPS spectra of N-FLG in the C1s, N1s and O1s regions, with the corresponding deconvolutions.

The C1s spectrum was fitted with seven peaks: a main peak at 284.6 eV assigned to the graphitic structure (sp^2), a peak at 285.5 eV attributed to C-C single bonds of defects on graphene structure (sp^3) and C=N double bond (resulting from nitrogen-doping), a peak at 286.3 eV related to C-O single bonds in alcohol and ether functionalities, a peak

at 287.1 eV due to C-N single bonds, two peaks at 287.9 and 288.8 eV assigned, respectively, to carbon-oxygen double bonds in ketones and quinones (C=O) and in carboxylic acid and ester functionalities (-COO) and a peak at 290.8 eV attributed to the characteristic shake-up satellite for the π-π*transition [43-45]. The O1s spectrum was fitted with two peaks at 530.7 and 532.5 eV, which can be ascribed to O=C double bond from ketone and quinone moieties and to O-C single bond from ether and phenol groups, respectively. These peaks also encompass contributions from carboxylic acid and ester groups and from the O-N bond (from nitrogen-doping) [43,46]. The N1s spectrum was fitted to four components: at 398.7 eV (pyridinic-N), 401.2 eV (pyrrolic-N), 403.0 eV (quaternary-N) and 405.1 eV (pyridinic-N-oxide) [31,44,47,48].

The total atomic content of each element on N-FLG sample was found to be 95.6 at.% of C, 2.1 at.% of N and 2.2 at.% of O. From the 2.1 at.% of N, pyrrolic-N and pyridinic-N constitute the major components, 43.0 and 37.8 at.%, respectively, followed by quaternary-N 12.7 at.% and pyridinic-N-oxide 6.4 at.%. The presence of oxygen can be attributed to the formation of surface functional groups created at the edges during acid treatment in air. XPS spectrum of undoped FLG (not shown) was also found to contain oxygen in the range (2-4 at.%).

The effect of doping on the structure of FLG was further confirmed from Raman spectra. Figure 3 shows the Raman spectra of doped and undoped FLG. For both doped and undoped FLG, the Raman spectrum is highly uniform over the whole sample. The undoped FLG shows a narrow G band confirming the presence of a well crystallized sp^2 carbon network. The D and D' bands are relatively high, that could be the result of defects at edges of smaller flakes. Eckmann *et al.* [49,50] have found that the intensity ratio of the D and D' peak is maximum (~ 13) for sp^3-defects, it decreases for vacancy-like defects (~ 7) and reaches a minimum for boundaries in graphite (~ 3.5). The ratio of D/D' (~ 2)

observed in our case corresponds to a grain size of ~ 10 nm for the undoped sample, which is in agreement with the TEM data (see Figure S1). A symmetric 2D band with 1.5 times the intensity of the G band is observed and the width of this band is similar to single layer graphene. This shows that the individual graphene layers are randomly stacked [36]. In contrast, the Raman spectrum of N-FLG shows a dramatic change as compared to the undoped sample. The G band is shifted from 1576 to 1592 cm^{-1} (16 cm^{-1}) and the D band and 2D bands are blue shifted by 17 and 6 cm^{-1} respectively. The 2D band is completely attenuated, even though the width of this band does not change. The blue shift in the G band frequency and the attenuation of the 2D band without broadening has been attributed to doping of the graphene lattice [31,51]. In fact, these changes could be attributed to Bernal staked multilayer graphene, but as in this case the staking is turbostratic, the attenuation of 2D band as compared to undoped FLG should come from doping effects. Both G and D bands are broadened by 3 to 4 times, indicating the large number of defects created during the nitrogen doping process. Nevertheless, the I_D/I_G values increase only slightly from 0.97 to 1.04 after doping. Such characteristics are typical of nitrogen doping as has been reported by other studies [52]. Therefore, we attribute the Raman spectral changes to nitrogen doping. We note that spectra of FLG containing oxygen functional groups produced by acid treatment did not show a G band shift. Hence, it appears that the change in the G band frequency is a direct consequence of the substitution of nitrogen in the graphene lattice.

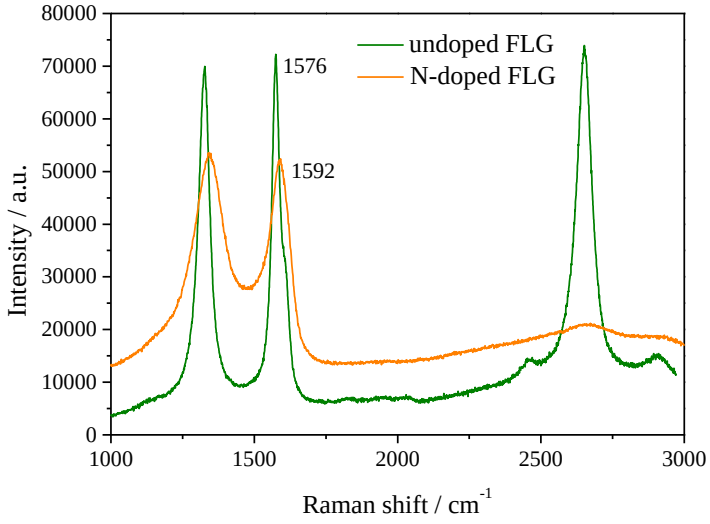

Figure 3. Raman spectra of undoped and N-doped FLG.

3.2 Electrochemical preparation and characterization of N-FLG@poly[1]

The CVs obtained during the 1st, 10th and 30th electrodeposition cycles of the N-FLG@poly[1] film are depicted in Figure 4 (a), along with the same electrodeposition cycles for pristine poly[1] film, for comparison. The CVs obtained in the complete films electrodepositions are shown in Figure S2 and the peak potential values are summarized in Table S1.

The CVs of the nanocomposite electrodeposition have similar electrochemical profiles to those of the pristine poly[1] film, despite a small shift of the anodic peaks for less negative potentials and of the cathodic peaks for more negative potentials. These results indicate that the presence of N-FLG did not changed the oxidative electropolymerization mechanism of poly[1]. Consequently, the two peaks observed in the first anodic half-cycle, at E_{pa} = 0.96 and 1.13 V are attributed to the [Ni(3-Mesalen)] monomer oxidation and subsequent formation of oligomer/polymer in the vicinity of the working electrode surface while, in the reverse scan, the peaks at E_{pc} = 0.68 and 0.18 V correspond to the reduction of the as-formed nanocomposite film. The anodic peak around

E_{pa} = 0.49 V, which appears in the second and subsequent scans, is attributed to the oxidation of the as-formed polymeric film [33,53].

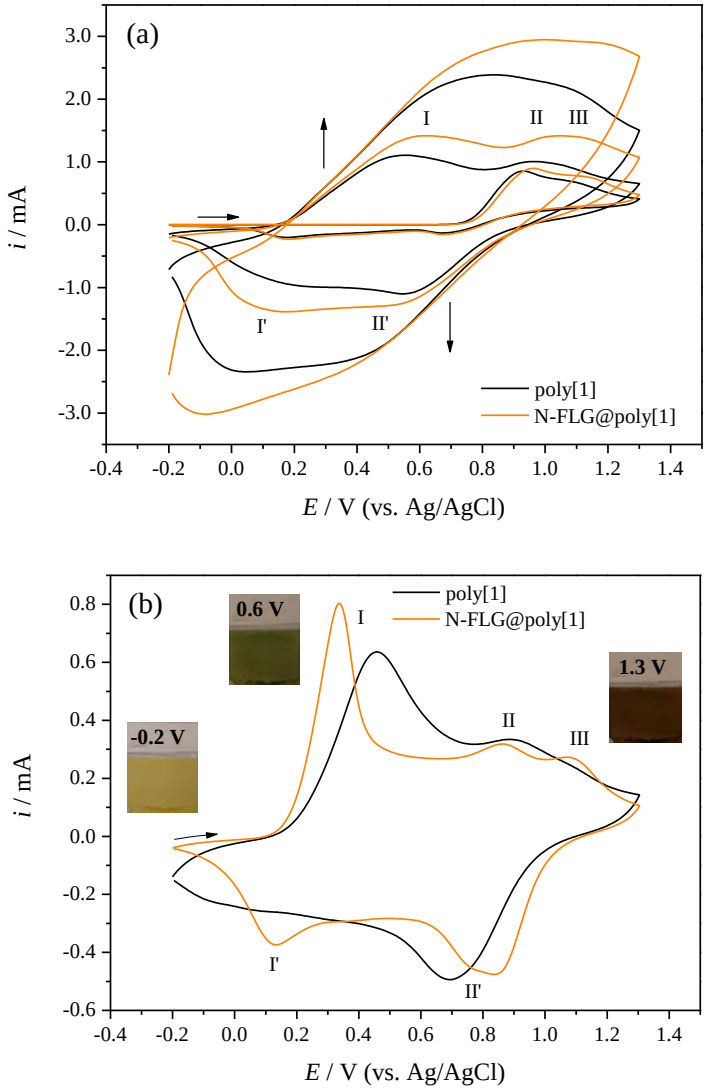

Figure 4. CVs obtained during (a) the 1st, 10th and 30th scans of electrodeposition and (b) the 3rd scan of the redox switching in 0.1 mol dm^{-3} $LiClO_4$/PC of representative N-FLG@poly[1] (Γ = 296 nmol cm^{-2}) and poly[1] (Γ = 180 nmol cm^{-2}) films; insets in (b) are films photographs in different oxidation states.

Moreover, the CVs of the nanocomposite show higher current intensities when compared to those of the pristine film (for the same cycle), which become more significant with the increasing number of electrodeposition cycles. This is attributed to

the larger electroactive surface area of the as-prepared nanocomposite film, resulting from the incorporation of the N-FLG in the polymeric matrix.

The CV obtained during the cycling (3rd scan) of the as-prepared N-FLG@poly[1] film in 0.1 mol dm^{-3} $LiClO_4$/PC, along with the CV of the pristine film, is depicted in Figure 4 (b). Figure S3 shows the CVs for film conditioning and Table S2 summarizes the peak potential values. The nanocomposite and pristine films have similar electrochemical responses although, in the former, the anodic and cathodic peaks are more well-defined and appear at less and more positive potentials, respectively, i.e. the peak potential separation is decreased. These observations suggest that the N-FLG@poly[1] film is more readily oxidized (and reduced) than the pristine film, i.e. more closely resembles a reversible system. This is attributed to the presence of N-FLG and its high electrical conductivity [29]. We infer that N-FLG enhances electron transport through the polymeric matrix, facilitating the polymer redox processes.

Figure 5 shows the electroactive surface coverage (Γ) profiles for nanocomposite and pristine films and the manner of their increase with the number of the electrodeposition cycles.

For thin films (prepared with 1 or 5 electropolymerization cycles), the N-FLG@poly[1] and the pristine poly[1] show similar Γ values, with Γ increasing linearly with the number of deposition cycles. However, as the number of cycles increases beyond 10, N-FLG@poly[1] shows higher apparent (i.e. electronically accessible on the experimental timescale) Γ values than the pristine film. This behaviour is similar to that observed for poly[1] doped with pristine graphene [34], although the Γ increase is more pronounced with N-FLG. These results are in agreement with the higher current intensities observed for the nanocomposite, as mentioned above, and provide indirect indication of the successful incorporation of the N-FLG into the poly[1] matrix. For films

prepared in the typical conditions employed in this work (at v = 0.100 V s^{-1} during 30 scans), Γ = 180 nmol cm^{-2} for pristine poly[1] and Γ = 296 nmol cm^{-2} for N-FLG@poly[1], where these values represent the populations accessible on the experimental timescale used.

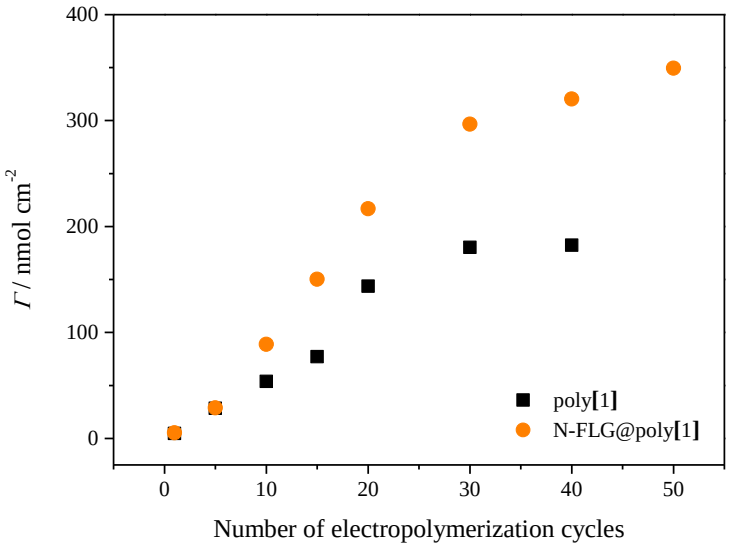

Figure 5. Plot of the (apparent, i.e. accessible) electroactive surface coverage, Γ, with the number of electropolymerization cycles for representative N-FLG@poly[1] and pristine films.

The visual inspection of the N-FLG@poly[1] film during its redox switching allowed to observe that the nanocomposite has similar EC behaviour to the pristine poly[1] [33]. In the inset in Figure 4 (b), photographs of the nanocomposite film in different oxidation states are presented, showing yellow (E = -0.2 V), green (E = 0.6 V) and russet (reddish-brown) (E = 1.3 V) colours at the different applied potentials.

3.3 Composition and morphology

The surface composition of N-FLG@poly[1] films in the reduced state (E = -0.2V) obtained by XPS revealed the presence of C, Ni, N, O and Cl elements, as expected. The

deconvoluted high-resolution XPS spectra for nanocomposite and pristine films, for comparison, are shown in Figures S4 and S5, in SI. The comparison between the two deconvoluted XPS spectra and the atomic ratios of the nanocomposite *vs* pristine film provides valuable information.

The C1s spectrum of N-FLG@poly[1] was deconvoluted into four components: a peak at 284.6 eV attributed to aromatic and aliphatic carbons of the *salen* moiety and to the structure of N-FLG, a peak at 285.9 eV associated with the C-O and C-N bonds of the *salen* coordination sphere and with the C-O single bonds in N-FLG, a peak with lower intensity at 286.9 eV assigned to C≡N from CH_3CN entrapped on the film and to C-N bonds of the N-FLG, and a peak at 289.3 eV related to the shake-up satellite of π-π*transitions due to the aromatic carbons of *salen* and N-FLG and that also has the contribution of C=O and –COO bonds of N-FLG [37,44].

The N1s spectrum of the nanocomposite was deconvoluted into four peaks at 399.4, 400.4, 401.3 and 403.4 eV. The first peaks are attributed to the nitrogen bonds of the ligand system and to pyridinic-N of the N-FLG, the peak at 401.3 eV is assigned to the N≡C bound of occluded CH_3CN and to pyrrolic-N of the N-FLG and the peak at 403.4 eV is associated to a shake-up phenomenon due to *salen* ligand and to quaternary-N and pyridinic-N-oxide of the N-FLG [31,37,44].

The deconvoluted O1s spectrum of the nanocomposite exhibits two peaks: one at 531.5 eV assigned to oxygen belonging to the coordination sphere of *salen* ligand and O=C bonds from N-FLG, and other at 533.1 eV attributed to the presence of ClO_4^- (from supporting electrolyte) occluded on polymeric films and to O-C bonds from N-FLG [37].

The Ni2p spectrum of the nanocomposite shows the characteristic peaks due to Ni coordinated to *salen* ligand in a formal +2 oxidation, which are assigned to: Ni $2p_{3/2}$ (855.3 eV), Ni $2p_{3/2}$ satellite (860.6 eV), Ni $2p_{1/2}$ (872.5 eV) and Ni $2p_{1/2}$ satellite (877.8

eV). The presence of peaks in the high resolution Cl2p region at 208.4 eV ($Cl2p_{3/2}$) and 210.0 eV ($Cl2p_{1/2}$) are consistent with the presence of ClO_4^- from supporting electrolyte within the nanocomposite film [37].

The deconvoluted XPS spectra of the pristine poly[1] show the typical peaks of the Ni-*salen* polymer, as described elsewhere for similar films [37]. The C1s spectrum was deconvoluted into four components: a peak at 284.6 eV attributed to aromatic and aliphatic carbons of *salen* ligand, a peak at 286.0 eV associated with C-O and C-N bonds of the *salen* moiety, a peak at 287.0 eV assigned to C≡N from CH_3CN and a peak at 289.4 eV related to the shake-up satellite of the π-π*transitions [37]. The N1s spectrum was deconvoluted into four peaks at 399.5, 400.5, 401.6 and 403.6 eV attributed to the nitrogen bonds of the ligand system, to the N≡C bound of occluded CH_3CN and to a shake-up phenomenon, respectively [37]. The deconvoluted O1s spectrum shows two peaks: one at 531.5 eV assigned to oxygen within the coordination sphere of the *salen* ligand, and another at 533.1 eV attributed to the presence of occluded ClO_4^- [37]. The peaks observed in the Ni2p spectrum are assigned to the $Ni2p_{3/2}$ (855.3 eV), $Ni2p_{3/2}$ satellite (860.6 eV), $Ni2p_{1/2}$ (872.5 eV) and $Ni2p_{1/2}$ satellite (877.8 eV). Features observed in the Cl2p spectrum are attributed to $Cl2p_{3/2}$ (208.3 eV) and $Cl2p_{1/2}$ (209.9 eV) from ClO_4^- [37].

Surface atom percentages obtained for the nanocomposite and pristine films are summarized in Table 1, from which we calculate the surface atom ratios.

Table 1: Surface atom percentages obtained by XPS and calculated atom ratios of relevant elements for poly[1] and N-FLG@poly[1] nanocomposite films, emersed in the in the reduced state (at E = -0.2 V).

Films	Atom %					Atom Ratios		
	Ni	C	N	O	Cl	N/Ni	O/Ni	Cl/Ni
poly[1]	3.1	70.8	6.7	16.9	2.5	2.2	5.4	0.8
N-FLG@poly[1]	2.6	67.3	6.4	20.5	3.3	2.5	7.9	1.3

The atom ratio N/Ni calculated for N-FLG@poly[1] is higher than of the expected value considering the [Ni(3-Mesalen)] chemical structure ($N/Ni_{theoretical}$ = 2.0). We rationalise this as being due to two factors, namely the trapping of CH_3CN in the nanocomposite matrix (see also the N1s peak at 401.3 eV in N1s nanocomposite spectrum) and the presence of N-FLG. In fact, for the nanocomposite, the N/Ni atom ratio is 12 % larger than for poly[1].

The O/Ni and Cl/Ni atomic ratios are also above than the expected values ($O/Ni_{theoretical}$ = 2.0), but their increase in a proportion ca. 1:4 (Cl:O) confirms that this is due to the trapping of ClO_4^- in the polymeric film, as typically observed for analogous systems [37]. In the nanocomposite, the O/Ni and Cl/Ni atomic ratios are greater by ca. 32% and 38 %, respectively, than in the pristine film, indicating more occluded ClO_4^-.

Figure 6 shows a SEM micrograph of the N-FLG@poly[1] film with the corresponding EDS spectrum at a selected region, identified as Z1.

In Figure 6 (a) it is possible identify a continuous layer with an irregular surface characteristic of the metal *salen*-type pristine films [33,53], which is blended with N-FLG fragments in certain regions (Z1). The micrograph shows that the poly[1] matrix extents over the N-FLG fragments and, thus, N-FLG is in fact occluded *within* poly[1], not merely *on* the surface of the film. The nature of the fragment was confirmed by EDS analysis in

the Z1 region (indicated in Figure 6 (b)). The elements predominantly detected were carbon and oxygen, which are characteristic of graphene flakes. Ni was also detected in low amounts and the absence of other elements typically observed in poly[1] confirms that the fragment is predominantly carbon-based, i.e. graphene. Note that the presence of N in FLG composition has been confirmed by XPS and chemical analysis, whereby its correspondent peak in EDS spectrum (expected at ca. 0.30-0.40 keV) should be overlapped by the very intense C peak or mixed with the spectrum noise, due to the low content of nitrogen in comparison with carbon. These results demonstrate the successful preparation of the N-FLG@poly[1] nanocomposite.

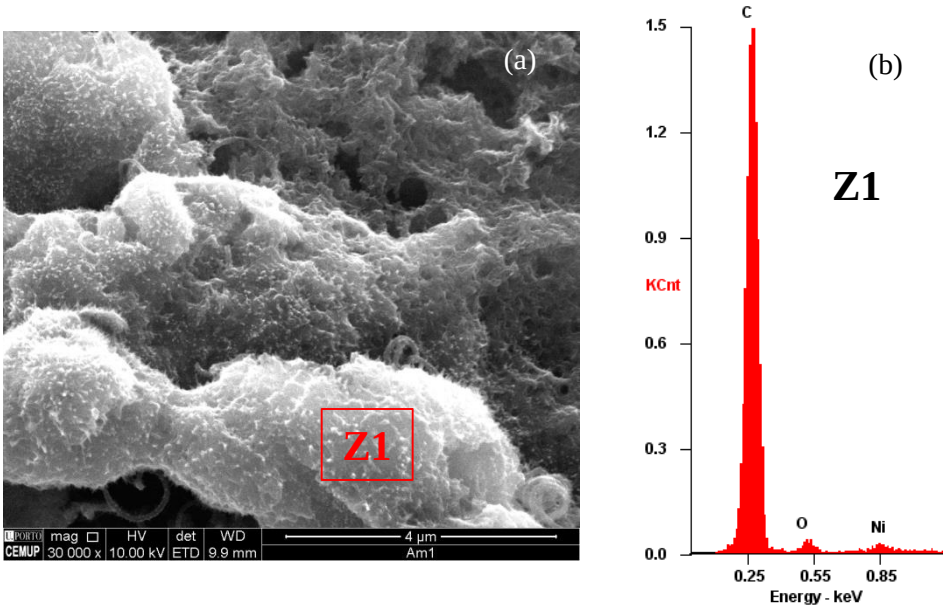

Figure 6. (a) Scanning electron micrograph and (b) EDS spectrum at specified zone (Z1) of N-FLG@poly[1] film.

3.4 *In situ* UV-Vis spectroscopy

Figure 7(a) depicts the absolute UV-Vis spectra acquired during the oxidation of the N-FLG@poly[1] nanocomposite film; for comparison, the equivalent spectra for

pristine poly[1] are depicted in Figure S6 (a) in SI. The spectra obtained during film reduction showed an inverse behaviour and were omitted for presentational clarity.

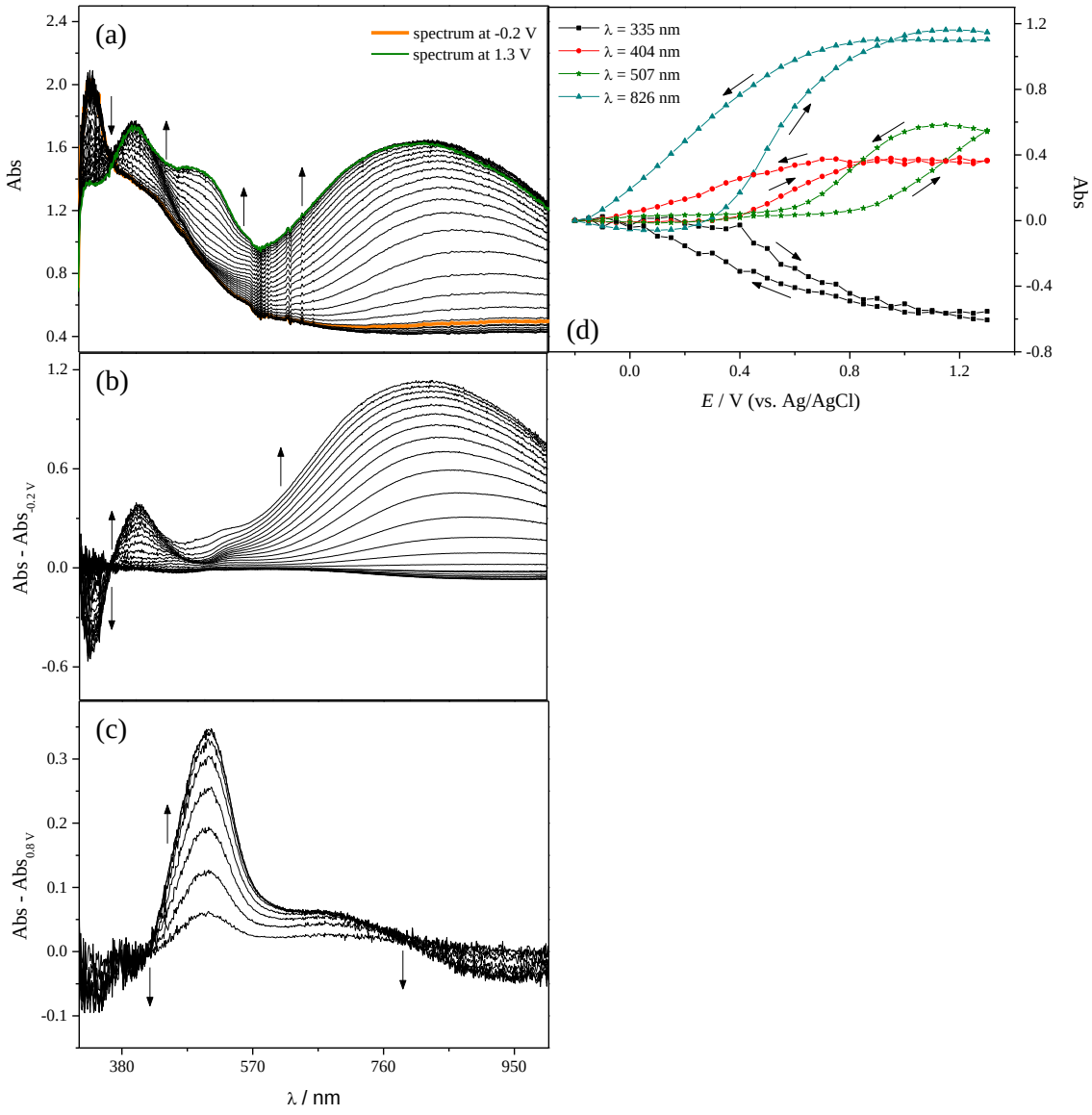

Figure 7. UV-Vis spectra of representative N-FLG@poly[1] (Γ = 296 nmol cm^{-2}) acquired during film oxidation in 0.1 mol dm^{-3} $LiClO_4$/PC: (a) absolute spectra, referenced to the electrolyte spectrum, (b) differential spectra from -0.2 to 0.8 V, referenced to the spectrum of neutral polymer (at E = -0.2 V), (c) differential spectra from 0.8 to 1.3 V, referenced to the spectrum of polymer at E = 0.8 V and (d) *Abs* vs. E plots of the electronic bands identified in absolute UV-Vis spectra, referenced to the spectrum at E = -0.2 V (arrows indicate scan direction).

The N-FLG@poly[1] spectra are very similar to those of the pristine film: both show four electronic bands. The electronic band profiles as function of applied potential are most readily appreciated in the differential spectra, relative to spectral responses at selected potentials. In the present instance, the reference points are the spectra at applied potentials of -0.2 V (fully reduced film) and 0.8 V (where the first oxidation stage is complete; see Figure 4(b)). The full spectral outcomes are shown in Figures 7(b) and (c) for the nanocomposite; the outcome of the control experiment, involving poly[1], is shown in Figures S6 (b) and (c). The absorbance *vs.* potential (*Abs vs. E*) profiles at the peak wavelengths are shown in Figure 7(d) for the nanocomposite and in Figure S6 (d) for the pristine polymer. These representations reveal that the nanocomposite and pristine films have similar electronic band behaviours, highlighting the band profiles characteristic of several metal *salen*-type films [37,38,54] and of the pristine poly[1] film [33].

The energies of the electronic bands for both films are summarised in Table 2. Molar extinction coefficients, ε, were estimated from the slopes of *Abs* vs. *Q* plots (Figure S7) using Equation 1.

Table 2: Electronic bands energy and molar extinction coefficients (ε) for pristine poly[1] and N-FLG@poly[1] films.

Film	**λ / nm (eV)**	**$\varepsilon \times 10^{-3}$ / cm^{-1} mol^{-1} dm^3**
poly[1]	332 (3.74)	3.86
	401(3.09)	2.16
	509 (2.44)	8.80
	818 (1.52)	5.26
N-FLG@poly[1]	335 (3.70)	3.17
	404 (3.07)	2.66
	507 (2.45)	7.78

	826 (1.50)	7.11

Taking into account the assertion of ligand-based film oxidation, supported by the ε-values and proposed for the pristine [33] and other similar poly[M(*salen*)] films [37,54], the polaronic model previously employed in the assignment of the electronic bands of metal *salen*-type films [33,37,38,54] can be used for band assignment, as follows. First, the band at λ = 332-335 nm is attributed to the intervalence transition and corresponds to the band gap (E_g = 3.74 and 3.70 eV for pristine and nanocomposite films, respectively). Second, the bands at λ = 401-404 nm (3.09-3.07 eV) and λ = 818-826 nm (1.52-1.50 eV) that appear during film oxidation, are attributed to transitions within the band gap, from the valence band to the antibonding and bonding polaron levels, respectively. Finally, the band at λ = 507-509 nm (2.45-2.44 eV) is assigned to the charge transfer (CT) transition between the metal and the oxidized ligand.

The data summarized in Table 2 reveal that the energies of the observed bands in the nanocomposite are very similar to those of the pristine film, showing that the incorporation of the N-FLG into the poly[1] matrix did not substantively change the metallopolymer electronic structure. However, the ε–values for the nanocomposite electronic bands are different from those of the pristine film. The nanocomposite electronic bands assigned to transitions within the band gap, at λ = 401-404 nm and λ = 818-826 nm showed, respectively, 19 % and 26% *increases*; conversely, for the CT band at λ = 507-509 nm, the ε–value *decreased* 12 %. Since the electronic bands associated with transitions within the band gap are associated with charge carriers within the film, the increase in the molar extinction coefficients is in line with the previous conclusions that the incorporation of N-FLG in the poly-*salen* matrix is providing alternative conductive pathways and thence improving overall charge transport [6]. Further, since

the CT band is associated with polymer over-oxidation and less stable oxidised states of poly-*salen* materials, the decrease of the corresponding ε–value is a very good outcome in that it points to increased film stability towards over-oxidation.

3.5 Electrochromic properties

The EC parameters for the N-FLG@poly[1] nanocomposite were determined in order to evaluate the effect of N-FLG incorporation. This characterization was performed for the yellow ↔ green colour change and using $LiClO_4$/PC as supporting electrolyte, since these conditions were found to be optimal for EC performance of the pristine film [33]. The EC parameters are representative for the typical nanocomposite films (Γ = 296 nmol cm^{-2}; for pristine poly[1] film Γ = 180 nmol cm^{-2}) employed in this work and might be a practical value.

The electrochemical stability of the N-FLG@poly[1] film was evaluated by chronoamperometry, monitoring the current intensity decay through 10 000 redox cycles, the equivalent of ≈ 12 days, after which the colour change was still visually perceptible. The chronoamperograms, Figure 8(a), show that, at the end of the experiment, the nanocomposite film only lost 2.7 % of charge, while the pristine poly[1] film lost 9.3% of the initial charge, which represents an improvement of 71.0 % in electrochemical stability. These observations are supported by very similar voltammetric profiles (peak potentials and current intensities) obtained for N-FLG@poly[1] film before and after the chronoamperometric study (see Figure S8 in SI).

In Figure 8(b) the chronoamperograms obtained during the first cycles for representative N-FLG@poly[1] and poly[1] films are compared. The nanocomposite film shows much faster switching times, τ = 11 and 9 s for oxidation (yellow to green transition) and reduction (green to yellow transition), respectively. These are substantive

improvements – by a factor of *ca.* 4 - over the corresponding switching times of $\tau = 49$ s and 31 s for oxidation and reduction of the corresponding pristine poly[1] film.

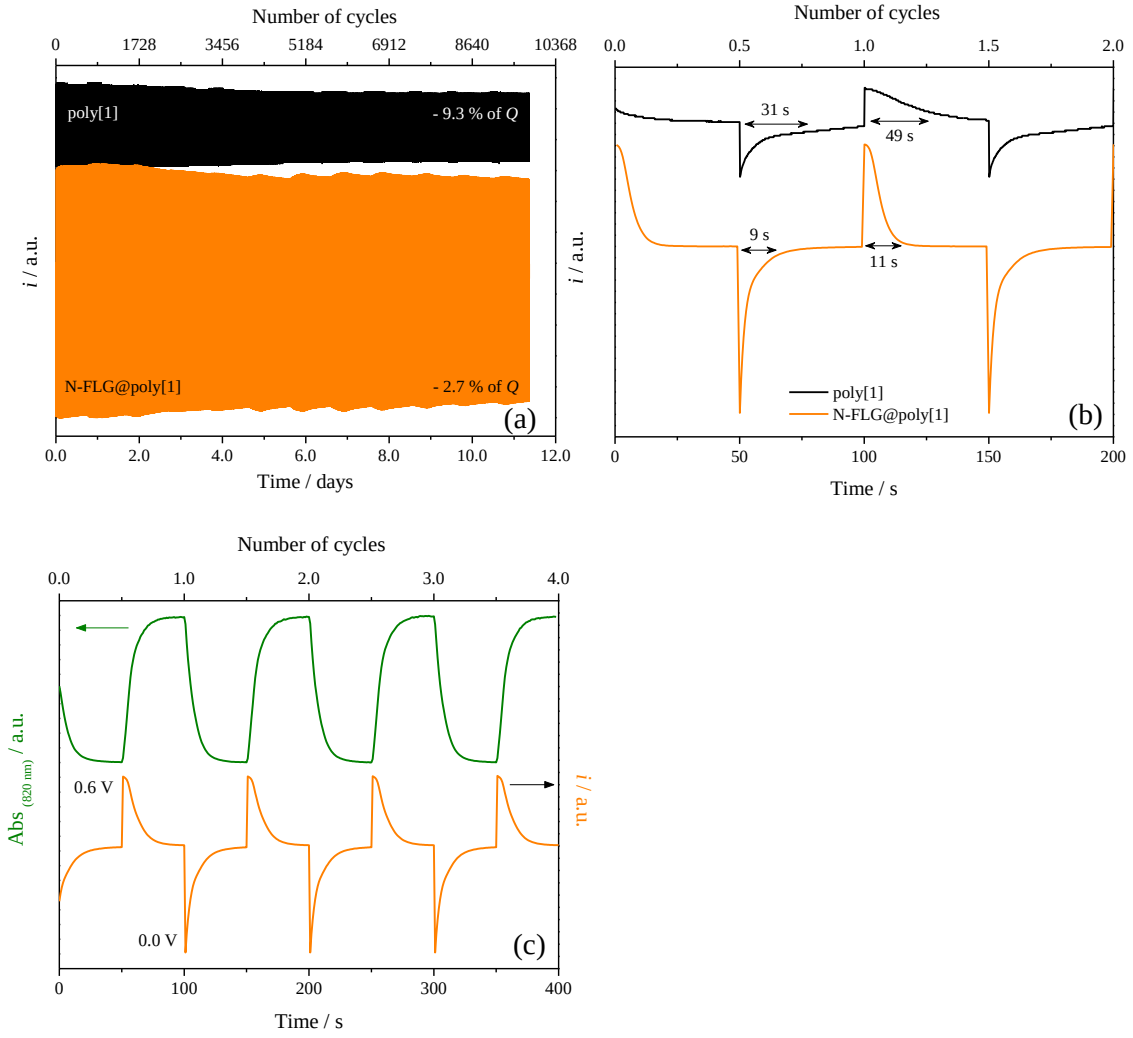

Figure 8. (a) Chronoamperograms of N-FLG@poly[1] and pristine poly[1] films in 0.1 mol dm^{-3} $LiClO_4$/PC, applying two potential steps of 50 s by redox cycle, with potential alternating between E = 0.0 V (yellow) and E = 0.6 V (green); (b) expansion of the chronoamperograms, showing the measured switching times; (c) single wavelength chronoamperograms/absorptograms obtained for N-FLG@poly[1] film during 4 redox cycles, at λ = 820 nm.

The asymmetry in the switching times observed for both polymer films with respect to the switching direction is rationalized on the basis of differences in conductivity of the

EC polymer in the initial state, in electric field strength, in (initial) film solvation and in mobile ion diffusion rates within the film, all of which are dependent on switching direction [55].

The optical contrast ΔT %, optical density changes ΔOD and colouration efficiencies η of the N-FLG@poly[1] nanocomposite (and of the pristine film for comparison) were evaluated by chronoabsorptometry (λ = 820 nm). The chronoamperograms/absorptograms are shown in Figure 8 (c) and the calculated data are summarized in Table 3.

Table 3: EC parameters: optical contrasts (ΔT %), changes of the optical density (ΔOD), charge requirements (Q_d) and colouration efficiencies (η) for pristine poly[1] and N-FLG@poly[1] nanocomposite in $LiClO_4$/PC supporting electrolyte, at λ = 820 nm.

Film	**ΔT %**	**ΔOD**	**Q_d / mC cm^{-2}**	**η / cm^2 C^{-1}**
poly[1]	22.1	0.86	9.06	95.4
N-FLG@poly[1]	35.9	0.99	9.11	108.9

The ΔT value increased from ΔT = 22.1 % in pristine poly[1] to 35.9 % in nanocomposite film (38 % improvement) and the ΔOD values, from ΔOD = 0.86 in pristine film to ΔOD = 0.99 for nanocomposite film (13 % improvement).

Similarly, N-FLG@poly[1] films exhibited higher colouration efficiency than for pristine film, η = 108.9 cm^2 C^{-1} vs. η = 95.4 cm^2 C^{-1}. For the nanocomposite film, the slight increase in charge requirement, in comparison to the pristine film (Q_d = 9.11 vs. 9.06 mC cm^{-2}) is compensated by the higher ΔOD value, resulting effectively in an enhancement of η value of 12 %.

It is worthwhile to compare the EC properties of N-FLG@poly[1] films with those of the nanocomposite prepared through the incorporation of graphene flakes (GF) into poly[1], [34]. On going from the nanocomposite prepared with GF to that prepared with N-FLG the switching times were decreased ≈ 50 % for oxidation and ≈ 25 % for reduction (for GF nanocomposite τ = 24 and 12 s for oxidation and reduction, respectively) and the electrochemical stability was improved ≈ 61 % (for GF nanocomposite charge loss of 7 % after 10 000 cycles).

The comparison of the EC properties of N-FLG@poly[1] films with those from original film and nanocomposite with GF, clearly evidences that EC properties benefit from graphene incorporation, but the specific N-doping of graphene is a very important added value for the final excellent results that were obtained.

The great improvements in EC parameters provided by the N-FLG incorporation maybe explained by the particular properties introduced by the nitrogen doping, which corresponds to graphene n-type doping. This originates an increase in electronic density that lead to higher electrical conductivity and creation of alternative conducting pathways, that allow a uniform and efficient current distribution and improve the overall (electron and coupled ion) charge transport behaviour. This is consistent with higher (accessible) electroactive site coverages in the nanocomposite, as result of the incorporation of the N-FLG [6]. Furthermore, we may speculate that the N-FLG incorporation into the poly-*salen* matrix also changes the packing of the polymer strands, creating a more porous structure that facilitates ion mobility required for charge compensation during the polymer redox process [28]; this aspect also must have been encouraging for the faster switching times and better electrochemical stability. It is noteworthy that N-FLG incorporation would appear have beneficial electronic and steric effects which,

respectively, facilitate electron and ion transport; since these are coupled (by electroneutrality), facilitating both is critical.

4. CONCLUSIONS

The new N-FLG@poly[1] nanocomposite was successfully prepared by *in situ* potentiodynamic electropolymerization of poly[1] in the presence of N-FLG, the latter being effectively produced using a cobalt ferrite spinel as catalyst and is characterized by uniform flakes with a nitrogen-doping of 2.1 at.%. The electrochemical characterization of the nanocomposite film revealed similar electrochemical profiles to that of pristine poly[1] film, but better defined peaks and higher current intensities were observed, which are associated with higher electroactive surface coverages. UV-Vis spectroscopy revealed that the incorporation of N-FLG did not change the basic electronic structure of poly[1] film, although more subtle influences were found on the molar extinction coefficients of the bands assigned to transitions within the band gap (at λ = 404 and 826 nm, increase of 19 and 26 %). These bands are associated with the charge carriers, and the observed changes are attributed to provision of alternative conducting pathways by N-FLG incorporation. The molar extinction coefficient of the CT band decreased (by 12 %) in the composite, a beneficial outcome since this band is associated with polymer over-oxidation (degradation) processes.

The as-prepared N-FLG@poly[1] nanocomposite showed excellent enhancement of all EC properties, compared with the pristine electroactive film. The incorporation of the N-FLG decreased the electrochemically induced degradation substantially, decreasing charge loss to only 2.7 % after ≈ 10 000 cycles (≈ 12 days). Simultaneously, the switching times diminished dramatically from τ = 31 s (49 s) for reduction (oxidation) of the pristine film to τ = 9 s (11 s) for the corresponding processes in the nanocomposite. The optical

contrast and colouration efficiency also show significant improvement, increasing from ΔT = 22.1 to 35.9 % and from η = 95.4 to 108.9 cm^2 C^{-1}, respectively, from pristine poly[1] to the nanocomposite film.

In summary, preparation of the graphene@poly[1] nanocomposite using N-doped graphene resulted in substantial enhancement of material EC performance, satisfying the primary goal of the study. In general terms, this is predominantly attributable to the extraordinary properties of N-doped graphene, based around the enhanced electronic conductivity of this n-type semiconductor material, but we also note advantageous structural changes that facilitate ion transport. The outcomes highlight the advantages of the N-FLG@poly[1] nanocomposite preparation which, together with the established benefits of N-doping of graphene, promise enhanced EC properties poly(Ni-*salen*) films.

ACKNOWLEDGMENTS

The work was funded by European Union and Fundação para a Ciência e a Tecnologia (FCT)/MEC under FEDER funds (POCI/01/0145/FEDER/007265) and Program PT2020 (UID/QUI/50006/2013). MPA (SFRH/BD/89156/2012) also thanks FCT for her PhD grant. MN thanks FEDER funds POCI/01/0145/FEDER/007265 and PT2020 UID/QUI/50006/2013 for her post-doctoral grant.

REFERENCES

[1] Ma LN, Zhao P, Wu WJ, Niu HJ, Cai JW, Lian YF, et al. RGO functionalised with polyschiff base: multi-chemical sensor for TNT with acidochromic and electrochromic properties. Polym Chem 2013;4(17):4746-54.

[2] Fu CP, Foo C, Lee PS. One-step facile electrochemical preparation of WO_3/graphene nanocomposites with improved electrochromic properties. Electrochim Acta 2014;117:139-44.

[3] Ko JH, Yeo S, Park JH, Choi J, Noh C, Son SU. Graphene-based electrochromic systems: the case of Prussian Blue nanoparticles on transparent graphene film. Chem Commun 2012;48(32):3884-6.

[4] Saxena AP, Deepa M, Joshi AG, Bhandari S, Srivastava AK. Poly(3,4-ethylenedioxythiophene)-Ionic Liquid Functionalized Graphene/Reduced Graphene Oxide Nanostructures: Improved Conduction and Electrochromism. ACS Appl Mater Interfaces 2011;3(4):1115-26.

[5] Rende E, Kilic CE, Udum YA, Toffoli D, Toppare L. Electrochromic properties of multicolored novel polymer synthesized via combination of benzotriazole and N-functionalized 2,5-di(2-thienyl)-1H-pyrrole units. Electrochim Acta 2014;138:454-63.

[6] Reddy BN, Deepa M, Joshi AG, Srivastava AK. Poly(3,4-Ethylenedioxypyrrole) Enwrapped by Reduced Graphene Oxide: How Conduction Behavior at Nano level Leads to Increased Electrochemical Activity. J Phys Chem C 2011;115(37):18354-65.

[7] Wei HG, Zhu JH, Wu SJ, Wei SY, Guo ZH. Electrochromic polyaniline/graphite oxide nanocomposites with endured electrochemical energy storage. Polymer 2013;54(7):1820-31.

[8] Xiong SX, Wei J, Jia PT, Yang LP, Ma J, Lu XH. Water-Processable Polyaniline with Covalently Bonded Single-Walled Carbon Nanotubes: Enhanced Electrochromic Properties and Impedance Analysis. ACS Appl Mater Interfaces 2011;3(3):782-8.

[9] Wei HG, Yan XR, Wu SJ, Luo ZP, Wei SY, Guo ZH. Electropolymerized Polyaniline Stabilized Tungsten Oxide Nanocomposite Films: Electrochromic Behavior and Electrochemical Energy Storage. J Phys Chem C. 2012;116(47):25052-64.

[10] Kuilla T, Bhadra S, Yao DH, Kim NH, Bose S, Lee JH. Recent advances in graphene based polymer composites. Prog Polym Sci 2010;35(11):1350-75.

[11] Qi XY, Tan CL, Wei J, Zhang H. Synthesis of graphene-conjugated polymer nanocomposites for electronic device applications. Nanoscale 2013;5(4):1440-51.

[12] Potts JR, Dreyer DR, Bielawski CW, Ruoff RS. Graphene-based polymer nanocomposites. Polymer 2011;52(1):5-25.

[13] Wang L, Lu XP, Lei SB, Song YH. Graphene-based polyaniline nanocomposites: preparation, properties and applications. J Mater Chem A 2014;2(13):4491-509.

[14] Lee T, Min SH, Gu M, Jung YK, Lee W, Lee JU, et al. Layer-by-Layer Assembly for Graphene-Based Multi layer Nanocomposites: Synthesis and Applications. Chem Mat 2015;27(11):3785-96.

[15] Wei D, Kivioja J. Graphene for energy solutions and its industrialization. Nanoscale 2013;5(21):10108-26.

[16] Liu Y, Wang HH, Zhou J, Bian LY, Zhu EW, Hai JF, et al. Graphene/polypyrrole intercalating nanocomposites as supercapacitors electrode. Electrochim Acta 2013;112:44-52.

[17] Zhou SP, Zhang HM, Zhao Q, Wang XH, Li J, Wang FS. Graphene-wrapped polyaniline nanofibers as electrode materials for organic supercapacitors. Carbon 2013;52:440-50.

[18] Chu CY, Tsai JT, Sun CL. Synthesis of PEDOT-modified graphene composite materials as flexible electrodes for energy storage and conversion applications. Int J Hydrog Energy 2012;37(18):13880-6.

[19] Zhao C, Gai PP, Liu CH, Wang X, Xu H, Zhang JR, et al. Polyaniline networks grown on graphene nanoribbons-coated carbon paper with a synergistic effect for high-performance microbial fuel cells. J Mater Chem A 2013;1(40):12587-94.

[20] Hou JX, Liu ZL, Zhang PY. A new method for fabrication of graphene/polyaniline nanocomplex modified microbial fuel cell anodes. J Power Sources 2013;224:139-44.

[21] Wang GQ, Xing W, Zhuo SP. The production of polyaniline/graphene hybrids for use as a counter electrode in dye-sensitized solar cells. Electrochim Acta 2012;66:151-7.

[22] Bo Y, Yang HY, Hu Y, Yao TM, Huang SS. A novel electrochemical DNA biosensor based on graphene and polyaniline nanowires. Electrochim Acta 2011;56(6):2676-81.

[23] Dong YP, Zhang J, Ding Y, Chu XF, Chen J. Electrogenerated chemiluminescence of luminol at a polyaniline/graphene modified electrode in neutral solution. Electrochim Acta 2013;91:240-5.

[24] Song ZP, Xu T, Gordin ML, Jiang YB, Bae IT, Xiao QF, et al. Polymer-Graphene Nanocomposites as Ultrafast-Charge and -Discharge Cathodes for Rechargeable Lithium Batteries. Nano Lett 2012;12(5):2205-11.

[25] Chang CH, Huang TC, Peng CW, Yeh TC, Lu HI, Hung WI, et al. Novel anticorrosion coatings prepared from polyaniline/graphene composites. Carbon 2012;50(14):5044-51.

[26] Sheng KX, Bai H, Sun YQ, Li C, Shi GQ. Layer-by-layer assembly of graphene/polyaniline multilayer films and their application for electrochromic devices. Polymer 2011;52(24):5567-72.

[27] Lu JL, Liu WS, Ling H, Kong JH, Ding GQ, Zhou D, et al. Layer-by-layer assembled sulfonated-graphene/polyaniline nanocomposite films: enhanced electrical and ionic conductivities, and electrochromic properties. RSC Adv 2012;2(28):10537-43.

[28] Xiong SX, Li ZF, Gong M, Wang XQ, Fu JL, Shi YJ, et al. Covalently Bonded Polyaniline and para-phenylenediamine Functionalized Graphene Oxide: How the Conductive Two-dimensional Nanostructure Influences the Electrochromic Behaviors of Polyaniline. Electrochim Acta 2014;138:101-8.

[29] Wood KN, O'Hayre R, Pylypenko S. Recent progress on nitrogen/carbon structures designed for use in energy and sustainability applications. Energy Environ Sci 2014;7(4):1212-49.

[30] Wang HB, Xie MS, Thia L, Fisher A, Wang X. Strategies on the Design of Nitrogen-Doped Graphene. J Phys Chem Lett 2014;5(1):119-25.

[31] Wang HB, Maiyalagan T, Wang X. Review on Recent Progress in Nitrogen-Doped Graphene: Synthesis, Characterization, and Its Potential Applications. ACS Catal 2012;2(5):781-94.

[32] Yang CH, Chen SM, Wang TL, Shieh YT. Electrochromic Characteristics of Nitrogen-Doped Graphene/TiO_2 Nanocomposite Electrodes. Electrochim Acta 2014;123:268-77.

[33] Nunes M, Araújo M, Fonseca J, Moura C, Hillman AR, Freire C. ACS Appl Mater Interfaces 2016;8(8):14231-43.

[34] Araújo M, Nunes M, Fonseca J, Moura C, Hillman AR, Freire C. J Phys Chem C.submitted.

[35] Freire C, de Castro B. Spectroscopic characterisation of electrogenerated nickel(III) species. Complexes with N_2O_2 Schiff-base ligands derived from salicylaldehyde. J Chem Soc-Dalton Trans 1998(9):1491-7.

[36] Bacsa RR, Camean I, Ramos A, Garcia AB, Tishkova V, Bacsa WS, et al. Few layer graphene synthesis on transition metal ferrite catalysts. Carbon. 2015;89:350-60.

[37] Fonseca J, Tedim J, Biernacki K, Magalhaes AL, Gurman SJ, Freire C, et al. Structural and electrochemical characterisation of Pd(*salen*)-type conducting polymer films. Electrochim Acta 2010;55(26):7726-36.

[38] Tedim J, Patricio S, Fonseca J, Magalhaes AL, Moura C, Hillman AR, et al. Modulating spectroelectrochemical properties of Ni(*salen*) polymeric films at molecular level. Synth Met 2011;161(9-10):680-91.

[39] Dale SM, Glidle A, Hillman AR. Spectroelectrochemical observation of poly(benzo-c-thiophene) n-doping and p-doping. J Mater Chem 1992;2(1):99-104.

[40] Schott M, Lorrmann H, Szczerba W, Beck M, Kurth DG. State-of-the-art electrochromic materials based on metallo-supramolecular polymers. Sol Energy Mater Sol Cells 2014;126:68-73.

[41] Beaujuge PM, Reynolds JR. Color Control in π-Conjugated Organic Polymers for Use in Electrochromic Devices. Chem Rev 2010;110(1):268-320.

[42] Ju MJ, Jeon IY, Kim JC, Lim K, Choi HJ, Jung SM, et al. Graphene Nanoplatelets Doped with N at its Edges as Metal-Free Cathodes for Organic Dye-Sensitized Solar Cells. Adv Mater 2014;26(19):3055-62.

[43] Fernandes DM, Freire C. Carbon Nanomaterial-Phosphomolybdate Composites for Oxidative Electrocatalysis. ChemElectroChem 2015;2(2):269-79.

[44] Ratso S, Kruusenberg I, Vikkisk M, Joost U, Shulga E, Kink I, et al. Highly active nitrogen-doped few-layer graphene/carbon nanotube composite electrocatalyst for oxygen reduction reaction in alkaline media. Carbon 2014;73:361-70.

[45] Dongil AB, Bachiller-Baeza B, Guerrero-Ruiz A, Rodriguez-Ramos I, Martinez-Alonso A, Tascon JMD. Surface chemical modifications induced on high surface area graphite and carbon

nanofibers using different oxidation and functionalization treatments. J Colloid Interface Sci 2011;355(1):179-89.

[46] Lipinska ME, Rebelo SLH, Pereira MFR, Gomes J, Freire C, Figueiredo JL. New insights into the functionalization of multi-walled carbon nanotubes with aniline derivatives. Carbon 2012;50(9):3280-94.

[47] Asedegbega-Nieto E, Perez-Cadenas M, Morales MV, Bachiller-Baeza B, Gallegos-Suarez E, Rodriguez-Ramos I, et al. High nitrogen doped graphenes and their applicability as basic catalysts. Diam Relat Mat 2014;44:26-32.

[48] Lin ZY, Waller GH, Liu Y, Liu ML, Wong CP. Simple preparation of nanoporous few-layer nitrogen-doped graphene for use as an efficient electrocatalyst for oxygen reduction and oxygen evolution reactions. Carbon 2013;53:130-6.

[49] Eckmann A, Felten A, Mishchenko A, Britnell L, Krupke R, Novoselov KS, et al. Probing the Nature of Defects in Graphene by Raman Spectroscopy. Nano Lett 2012;12(8):3925-30.

[50] Lee JE, Ahn G, Shim J, Lee YS, Ryu S. Optical separation of mechanical strain from charge doping in graphene. Nat Commun 2012;3:8.

[51] Beams R, Cancado LG, Novotny L. Raman characterization of defects and dopants in graphene. J Phys-Condes Matter. 2015;27(8):26.

[52] Zhang CH, Fu L, Liu N, Liu MH, Wang YY, Liu ZF. Synthesis of Nitrogen-Doped Graphene Using Embedded Carbon and Nitrogen Sources. Adv Mater 2011;23(8):1020-4.

[53] Tedim J, Goncalves F, Pereira MFR, Figueiredo JL, Moura C, Freire C, et al. Preparation and characterization of poly Ni(*salen*)(crown receptor) /multi-walled carbon nanotube composite films. Electrochim Acta 2008;53(23):6722-31.

[54] Vilas-Boas M, Freire C, de Castro B, Christensen PA, Hillman AR. Spectroelectrochemical characterisation of poly Ni(saltMe) -modified electrodes. Chem-Eur J 2001;7(1):139-50.

[55] Amb CM, Dyer AL, Reynolds JR. Navigating the Color Palette of Solution-Processable Electrochromic Polymers. Chem Mat 2011;23(3):397-415.